SF2A 2023
M. N'Diaye, A. Siebert, N. Lagarde, O. Venot, K. Baillié, M. Béthermin, E. Lagadec, J. Malzac, J. Richard (eds)

MULTIWAVELENGTH OBSERVATIONS OF THE EXO-COMETARY DUST AROUND β PICTORIS.

P. Priolet[1], J.-C. Augereau[1], J. Milli[1], A. Matter[2] and J.-B. Le Bouquin[1]

Abstract. Since the discovery of its edge-on debris disk in 1984, β Pictoris has become a laboratory for studies on planet formation and planet-disk interactions, especially around the outer disk (from $\sim$ 10 au to $\sim$ 100 au). Nevertheless, the inner region ($<$ 4 au) remains fairly unconstrained. VLTI/PIONIER observations first revealed the presence of a small circumstellar emission in the H-band which is probably due to hot dust in the inner regions of the system.

We present in this study the first detection of the circumstellar emission from hot dust around β Pictoris in the L-band using VLTI/MATISSE. We also present preliminary results showing the presence of spatial information in the interferometric fringe visibility data, supporting previous models which suppose that the hot dust is confined close to the sublimation distance ($\sim$0.1–0.2 au).

Keywords:
debris disk, exozodiacal dust, interferometry, VLTI, β Pictoris

1 Introduction

β pictoris (HD 39060, HIP 27321) is a classic example of a young planetary system. Its host star is a young ($18.5^{+2.0}_{-2.4}$ Myr Miret-Roig et al. 2020), A6V type, main-sequence star. Its edge-on, cold debris disk located at tens to hundreds of astronomical units (au) was discovered in 1984 (Aumann 1984; Smith & Terrile 1984) and since then it has been thoroughly studied in search of planets. As of right now, two planets have been detected: β Pictoris b (semi-major axis $\sim$10 au, Lagrange et al. 2009, 2010) and β Pictoris c (semi-major axis $\sim$3 au, Lagrange et al. 2019). An excess circumstellar emission was also detected in the H-band representing $1.37 \pm 0.16\%$ of the photospheric emission (Defrère et al. 2012a). This excess has been attributed to hot dust in the inner regions of the debris disk, inside the orbits of the detected exoplanets.

To study in depth the properties of the hot and warm dust in the inner parts of this system, we propose to combine VLTI/PIONIER observations in the H-band with VLTI/MATISSE observations in the L-band. We present here the results of these near- and mid-infrared interferometric observations, including the first detection of an L-band excess in this system, as well as preliminary results indicating that valuable information on the dust location might be present in the data.

2 Detection of circumstellar emission

2.1 Observations

Multiwavelength interferometric observations of β pic were obtained in October 2022 using VLTI/MATISSE* in the L-band (Lopez et al. 2022) and VLTI/PIONIER† in the H-band (Le Bouquin et al. 2011). These observations were taken using the small configuration of the AT array at the VLTI and they were interleaved with observations of reference stars to calibrate the instrumental effects in the observed quantities. These calibrators were chosen close to β Pic both in terms of position and magnitude. In this study we also use archival data taken with

[1] Univ. Grenoble Alpes, CNRS, IPAG, F-38000 Grenoble, France
[2] Université Côte d'Azur, Observatoire de la Côte d'Azur, CNRS, Laboratoire Lagrange, France
*Program ID: 110.246D.003
†Program ID: 110.246D.001

PIONIER (H-band, 3 data sets [‡]) and MATISSE (L-band, 3 data sets [§]). For information on the H-band archival data obtained with PIONIER, refer to Ertel et al. (2014, 2016).

We focus here on the interferometric fringe squared visibilities (V^2) and not on the closure phase since it is close to 0 for all the datasets used. This however, allows us to rule out a bright companion in the FOV of the instrument.

2.2 Method

To search for circumstellar emission, we compare our data sets to the expected squared visibilities (V^2) of a purely photospheric model. For this stellar model we use the analytical model for a limb darkened photosphere by Hanbury Brown et al. (1974) using the linear H- and LM-band limb-darkening coefficients from Claret et al. (1995) and the stellar angular diameter calculated in Defrère et al. (2012b) using surface brightness relations (SBR, see Kervella et al. 2004) which give a limb darkened angular diameter $\theta_{LD} = 0.712 \pm 0.010$ mas. We see that both the MATISSE L-band and PIONIER H-band squared visibilities $V^2(B)$ show a deficit with respect to the stellar squared visibility $V^2_\star(B)$. This implies that an object is at least partially resolved in the FOV of the instruments.

First, we assume that this emission is homogeneous and over-resolved for the shortest baselines (ie: $V_{\rm CSE}$ close to $0, \forall B$, where $V_{\rm CSE}$ is the visibility of the circumstellar emission), an assumption which is commonly used in such studies (e.g. Ertel et al. 2014, 2016; Absil et al. 2021). This approximation, combined with the fact that the extended emission is faint relative to the star, strongly simplifies our approach (since we do not have to model the spatial distribution of the dust) and can lead to reasonable results as shown by Absil et al. (2009) and Defrère et al. (2011). In this case, the observed squared visibility $V^2(B)$ can be expressed as:

$$V^2(B) \simeq (1-f)^2 V^2_\star(B) \tag{2.1}$$

where $V_\star$ is the stellar visibility and f is the flux ratio between the circumstellar emission and the total emission (photospheric + circumstellar). We also suppose that the flux ratio f does not depend on the wavelength for a given band, which allows us to fit all spectral channels together. We then do a least squares minimization to find the parameter f.

2.3 Results

MATISSE : we detect the circumstellar emission in all the L-band data taken with MATISSE (including in archival data). The preliminary measured flux ratios f are : $2.36 \pm 0.42\%$, $2.37 \pm 0.27\%$, $2.52 \pm 0.08\%$ and $1.3 \pm 0.37\%$ for the following dates of observations, 08/01/2021, 16/01/2021, 28/01/2021 and 14/10/2022 respectively. It is to be noted that the 08/01/2021 dataset was taken using the UT array while the others were taken using the AT array.

PIONIER : we also detect circumstellar emission in the H-band data taken with PIONIER. We measure a preliminary flux ratio f of $1.6 \pm 0.11\%$ for the 2022 data. We repeated this methodology on already published archival data (Ertel et al. 2016) to confirm correct data processing and ensure homogeneity. We find that our values are consistently larger than the archival ones (see Fig. 1); this could be due in part to different calibration procedures between the data used in the study and the archival data we retrieved.

[‡]Program IDs: 088.C-0266(A), 090.C-0526(A) and 094.C-0232(A)
[§]Program IDs: 106.21Q8.006, 106.21Q8.004 and 106.21Q8.001

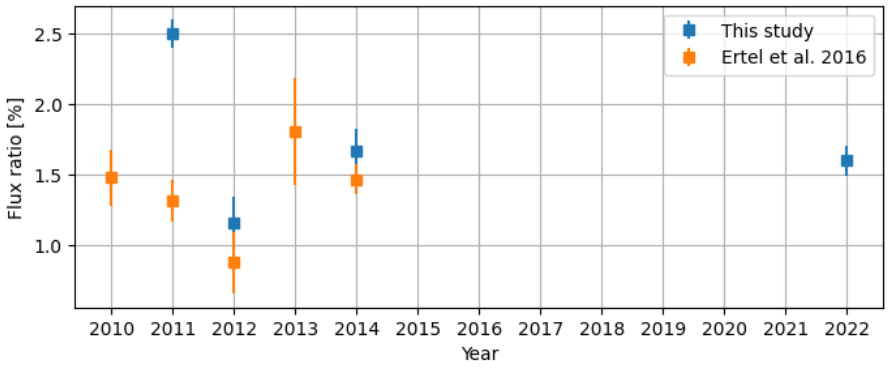

Fig. 1. Archival flux ratios from Ertel et al. (2016) compared to this study's estimates (VLTI/PIONIER data, H-band).

3 Spatial information

As hinted in Absil et al. (2021), approximating the circumstellar emission as homogeneous and over-resolved might lead to a miss estimation of the flux ratio. We therefore set out to test the presence of spatial information in the data by comparing it to the interferometric fringe visibilities of a geometrical model of an inclined flat ring.

3.1 Method

As in the previous section we use the analytical model for a limb darkened photosphere from Hanbury Brown et al. (1974) and we add a circumstellar emission in the form of a flat homogeneous geometrical ring. The visibility of such an object is analytical and allows for fast model fitting to the data. The free parameters of this model are: the internal radius ($r_{\rm in}$), the external radius (which we parametrize by a factor A such that $r_{\rm out} = A \times r_{\rm in}$ where $r_{\rm out}$ is the external radius), the inclination (i, such that $i = 0°$ for a pole-on disk and $i = 90°$ for edge-on), the position angle (PA) and finally the ratio between the flux of the flat ring and the total flux (f).

We then use an MCMC algorithm to fit this model to the dataset and extract the most likely parameters given our data set (supposing that this is a valid model for the circumstellar emission). This approach was employed for each of the PIONIER and MATISSE datasets separately.

3.2 Results

The free parameters remain unconstrained for most datasets; however, for certain datasets we find convergence of the free parameters (we do seem to constrain fairly well the internal radius), although some parameters are degenerated. One of the possible models has the same position angle (PA) as that of the external disk (29.5°, Boccaletti et al. 2009). We therefore decided to fix the PA of our model to that of the external disk to lift some of the degeneracies. As an example, the marginalized posterior probabilities for each parameter for the MATISSE dataset from 08/01/2021 when fixing the PA to 29.5° are shown in Figure 2.

These preliminary results show that thinner rings are preferred (small A values) and that the internal radius of the ring is close to the sublimation radius of both carbonaceous grains ($\sim$ 0.18 au for 10 nm-sized grains, $\sim$ 0.06 au for 1 μm-sized grains and $\sim$ 0.08 au for 1 mm-sized grains) and astronomical silicates ($\sim$ 0.23 au for 10 nm-sized grains, $\sim$ 0.17 au for 1 μm-sized grains and $\sim$ 0.13 au for 1 mm-sized grains).

It is also interesting to note that the fitted flux ratio in Figure 2 is higher than the one found in section 2.3.

4 Conclusions and discussion

This article presents preliminary work on the exozodi of β Pictoris. We show the detection of circumstellar emission in new H-band data and in the L-band data. This is the first time that the hot dust around β Pictoris is detected in the L-band and only one detection has been published so far with MATISSE in the L-band (κ

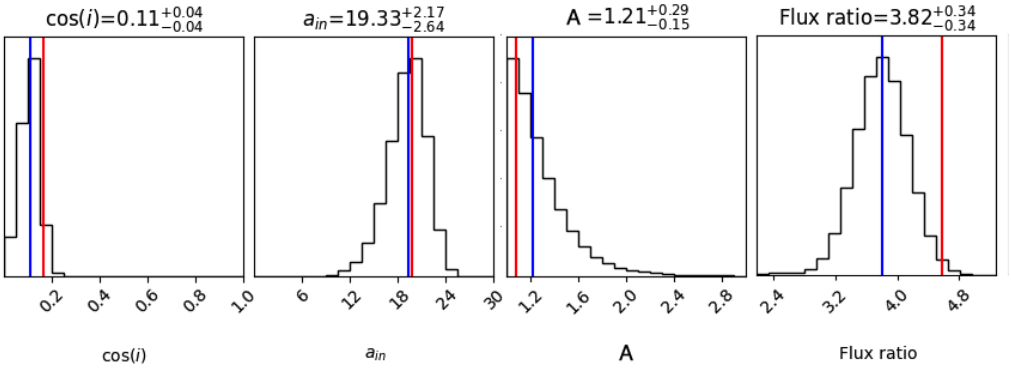

Fig. 2. Marginalized posterior probabilities for the free parameters using an archival MATISSE dataset (08/01/2021). The internal diameter of the ring ($a_{\rm in} = 2 \times r_{\rm in}$) is in mas and the flux ratio in % of the total flux. For more details on the definition of these parameters see section 3.1. The red lines represent the best fit values while the blue lines represents the median values of the posterior distribution.

Tuc Kirchschlager et al. 2020). In addition to the detection and measurement of the excess in the L- and H-bands, we indicate the possible presence of spatial information in these data sets. This could help alleviate a common degeneracy in SED modeling where smaller grains further from the star (including grains out of thermal equilibrium) have the same emission profile as larger grains closer to the star.

Since β Pic is viewed edge-on, a flat ring model might not be the best to reproduce the observed visibilities; this might lead to a best fitting model that is less inclined (less edge-on) than the actual dust to correctly reproduce the visibility signatures. A more detailed analysis is in preparation to take this effect into account.

This work was founded by the EPOPEE (Etude des POussières Planétaires Et Exoplanétaires) project supported by the French Planetology National Program (Programme National de Planétologie, PNP) and the Origin of life project supported by the Université Grenoble Alpes.

References

Absil, O., Marion, L., Ertel, S., et al. 2021, A&A, 651, A45
Absil, O., Mennesson, B., Le Bouquin, J.-B., et al. 2009, ApJ, 704, 150
Aumann, H. H. 1984, in Bulletin of the American Astronomical Society, Vol. 16, 483
Boccaletti, A., Augereau, J. C., Baudoz, P., Pantin, E., & Lagrange, A. M. 2009, A&A, 495, 523
Claret, A., Diaz-Cordoves, J., & Gimenez, A. 1995, A&AS, 114, 247
Defrère, D., Absil, O., Augereau, J. C., et al. 2011, A&A, 534, A5
Defrère, D., Lebreton, J., Le Bouquin, J. B., et al. 2012a, A&A, 546, L9
Defrère, D., Lebreton, J., Le Bouquin, J. B., et al. 2012b, A&A, 546, L9
Ertel, S., Absil, O., Defrère, D., et al. 2014, A&A, 570, A128
Ertel, S., Defrère, D., Absil, O., et al. 2016, A&A, 595, A44
Hanbury Brown, R., Davis, J., Lake, R. J. W., & Thompson, R. J. 1974, MNRAS, 167, 475
Kervella, P., Thévenin, F., Di Folco, E., & Ségransan, D. 2004, A&A, 426, 297
Kirchschlager, F., Ertel, S., Wolf, S., Matter, A., & Krivov, A. V. 2020, MNRAS, 499, L47
Lagrange, A. M., Bonnefoy, M., Chauvin, G., et al. 2010, Science, 329, 57
Lagrange, A. M., Gratadour, D., Chauvin, G., et al. 2009, A&A, 493, L21
Lagrange, A. M., Meunier, N., Rubini, P., et al. 2019, Nature Astronomy, 3, 1135
Le Bouquin, J. B., Berger, J. P., Lazareff, B., et al. 2011, A&A, 535, A67
Lopez, B., Lagarde, S., Petrov, R. G., et al. 2022, A&A, 659, A192
Miret-Roig, N., Galli, P. A. B., Brandner, W., et al. 2020, A&A, 642, A179
Smith, B. A. & Terrile, R. J. 1984, Science, 226, 1421